BULLETIN OF THE POLISH ACADEMY OF SCIENCES
TECHNICAL SCIENCES, Vol. 69(5), 2021, Article number: e138971
DOI: 10.24425/bpasts.2021.138971



# Structure and properties of suction-cast Pr-(Fe, Co)-(Zr, Nb)-B rod magnets

**Katarzyna PAWLIK***

Department of Physics, Faculty of Production Engineering and Materials Technology, Częstochowa University of Technology, Al. Armii Krajowej 19, 42-200 Częstochowa, Poland

**Abstract.** The rod specimens were produced from $Pr_9Fe_{50+x}Co_{13}Zr_1Nb_4B_{23-x}$ (x = 0, 5, 8) alloys using the suction-casting technique. Subsequent devitrification annealing of those samples resulted in the change of their phase structure and magnetic properties. For annealed specimens of all investigated compositions, the Rietveld analyses of X-ray diffractions have shown the presence of three crystalline phases: the hard magnetic $Pr_2Fe_{11.2}Co_{2.8}B$, soft magnetic α-Fe, and paramagnetic $Pr_{1+x}Fe_4B_4$, which have precipitated within the amorphous matrix. This technique allowed us to determine the weight fractions of constituent phases. Furthermore, the microstructural changes with the alloy composition were observed. Magnetic measurements of annealed rods allowed us to calculate the switching field distributions (SFD) and δM plots in order to determine the strength and character of magnetic interactions between grains of constituent phases.

**Key words:** bulk metallic glasses; bulk nanostructured magnets; RE-Fe-B magnets; miniature magnets.

## 1. INTRODUCTION

Permanent magnets based on the Re-Fe-B alloys are extensively used in various areas of technical applications, especially in electrical motors and actuators [1]. In order to reduce the sizes of such devices, new processing techniques must be applied. Application of suction-casting in processing miniature magnets of various shapes seems to be a promising method, facilitating cutting the manufacturing costs due to the reduction of time and energy consumption in the development of the nanocrystalline microstructure. Although this method enables us to obtain nanocrystalline miniature magnets in a single-stage process [2], it is rather difficult to control the magnetic properties of specimens of various shapes. Some of the RE-Fe-B alloys containing 9 at.% of RE (where RE = Nd, Pr, Dy) can be produced as partly or fully crystalline specimens directly by rapid solidification techniques. To obtain nanocrystalline samples doping of the base alloy with Zr, Ti, C, and Nb [2–5] was used. However, a more efficient approach to the tailoring of the microstructure and magnetic properties involves suitable annealing of the glassy precursor [6]. Two main factors determine the possibility of obtaining bulk glassy samples. The crucial one is the glass-forming ability (GFA) of the alloy itself. The second just as important is the critical cooling rate that can be reached with the use of specific applied equipment. A lot of work has been done in order to improve the GFA of RE-Fe-B alloys. It was shown that the addition of Nb, as well as an increase in the B content in the alloy composition, improve the GFA of the alloy [5–7]. Furthermore, doping with Zr and Nb causes the microstructure refinement of the RE-Fe-B magnets and, thus, can enhance the magnetic properties of the annealed specimens [8–10]. As was reported in [7], the appropriate setting of the composition for the $Fe_{67}Co_{9.4}Nd_{3.1}Dy_{0.5}B_{20}$ alloy led to an improvement of the GFA that allowed processing of the fully glassy rods with diameters up to 0.5 mm. A further change of composition and addition of Zr facilitated casting 1-mm diameter amorphous rods and up to 3-mm outer diameter tubes for the $Fe_{61}Co_{13.5}Zr_1Pr_{3.5}Dy_1B_{20}$ alloy [11]. However, a small amount of RE elements in the chemical composition caused the formation of a relatively low fraction of the $RE_2Fe_{14}B$ phase. For this reason, such magnets reveal rather moderate magnetic parameters [12]. We have shown in our previous studies on rapidly solidified plates of various thicknesses produced for $Pr_9Fe_{50+x}Co_{13}Zr_1Nb_4B_{23-x}$ (x = 0, 2, 5, 8) alloys that boron content greatly influences the GFA. In the case of the $Pr_9Fe_{50}Co_{13}Zr_1Nb_4B_{23}$ alloy, the 0.5-mm thick plates were fully amorphous while 1-mm plates were slightly crystalline and only one very low-intensity diffraction peak was detected [6, 13]. However, for alloys of lower B content, the suction cast plates were all crystalline in as-cast state. Furthermore, the critical cooling rate attainable for specific production equipment depends on the sample geometry [14]. The changes in the microstructure and magnetic properties with the sample shape were shown for the $Pr_9Fe_{52}Co_{13}Zr_1Nb_4B_{21}$ alloy [15].

The aim of the present work was to study the influence of the Fe to B ratio on the GFA as well as on the phase constitution, microstructure, and magnetic properties of the 1-mm diameter rods of $Pr_9Fe_{50+x}Co_{13}Zr_1Nb_4B_{23-x}$ (x = 0, 5, 8) alloys in the as-cast state and those subjected to annealing. Preliminary analysis of magnetic parameters has shown that optimal magnetic

*e-mail: katarzyna.pawlik@pcz.pl

Manuscript submitted 2021-02-26, revised 2021-06-26, initially accepted for publication 2021-07-31, published in October 2021

parameters were obtained for samples annealed at 983K. Therefore, in the present work, the detailed studies of rod samples annealed at this temperature were presented.

## 2. SAMPLES PREPARATION AND EXPERIMENTAL METHODS

The alloys of nominal compositions $Pr_9Fe_{50+x}Co_{13}Zr_1Nb_4B_{23-x}$ (x = 0, 5, 8) were produced by the arc-melting technique. For this purpose, the high purity elements, and pre-alloyed Fe–B were used. The process was carried out under the Ar atmosphere in order to prevent oxidation. The rapidly solidified 1-mm diameter rods were produced by suction-casting, using the procedure described in [15, 16]. The annealing was carried out at 983 K for 5 minutes in order to obtain the nanocrystalline microstructure and induce hard magnetic properties.

The phase constitution was determined using X-ray diffractometry (XRD). The XRD scans were measured using a Bruker D8 Advanced diffractometer equipped with a Cu tube. The CuKα radiation was separated using a Ni filter on the detector site of the goniometer. The specimens were crushed to powder in order to obtain XRD data representative for the entire volume of each specimen. After the qualitative phase identification, the Rietveld analysis of the XRD spectra was carried out. Prior to the analysis of studied samples, the instrument calibration using $LaB_6$ NIST 660 standard reference material was performed in order to determine the instrument peak profile. In the Rietveld analysis of the standard sample, the modified Thompson-Cox-Hastings (TCHZ) (pseudo-Voigt) function was used to generate phase peaks and to refine the emission profile (EM) of the instrument. The calculated TCHZ function and EM parameters were used for further analysis of the studied samples. For all investigated specimens, the background profile was fitted by the 5th order Chebyshev polynomials. The weight fractions of the amorphous phase and crystalline phases were calculated using the Rietveld refinement in which the partially or not known crystal structures method (the Rietveld-PONKCS method) was employed.

The microstructure was examined by the transmission electron microscopy (TEM).

Magnetic properties were measured at a room temperature, using the LakeShore 7307 VSM magnetometer in external magnetic field up to 2 T. The measurement of the recoil curves for the initially saturated and for initially demagnetized specimens allowed us to calculate the switching field distributions (SFD) and δM plots.

## 3. RESULTS AND DISCUSSION

X-ray diffraction patterns measured for 1-mm diameter rods in as-cast state and those subjected to annealing at 983K for 5 min for all investigated alloys are shown in Fig. 1. One must consider the fact that it is very difficult to unambiguously identify the component phases in the multiphase materials of the nanocrystalline structure. The reason for that is a strong overlap of closely situated peaks coming from different phases. Additionally, those peaks are widened and have lower intensities due to the nanocrystalline structure. Therefore, in some cases, they might be indistinguishable or create cumulative peaks in the X-ray diffraction spectrum. The Rietveld refinement was performed based on the model that assumed a presence of hard magnetic $Pr_2(Fe, Co)_{14}B$, paramagnetic $Pr_{1+x}Fe_4B_4$, and in some cases soft magnetic α-Fe crystalline phases. The detailed procedure used in the quantitative analysis was presented in [6, 12]. Especially, the Rietveld-PONKCS studies allowed us to determine the phase constitution including the weight fractions of the amorphous and crystalline phases as well as to estimate the crystal sizes of the investigated rods. In the analysis, the amorphous phase was represented by a group of peaks (peaks phase). The value of the ZMV parameter for such a phase was calculated from the XRD measurement carried out on the mixture of powders made of the phase of interest and the standard α-Fe of known weight ratio. The exact procedure was described in [17]. The calculated weight fractions of constituent phases, the crystallite sizes, and the refined cell parameters of the crys-

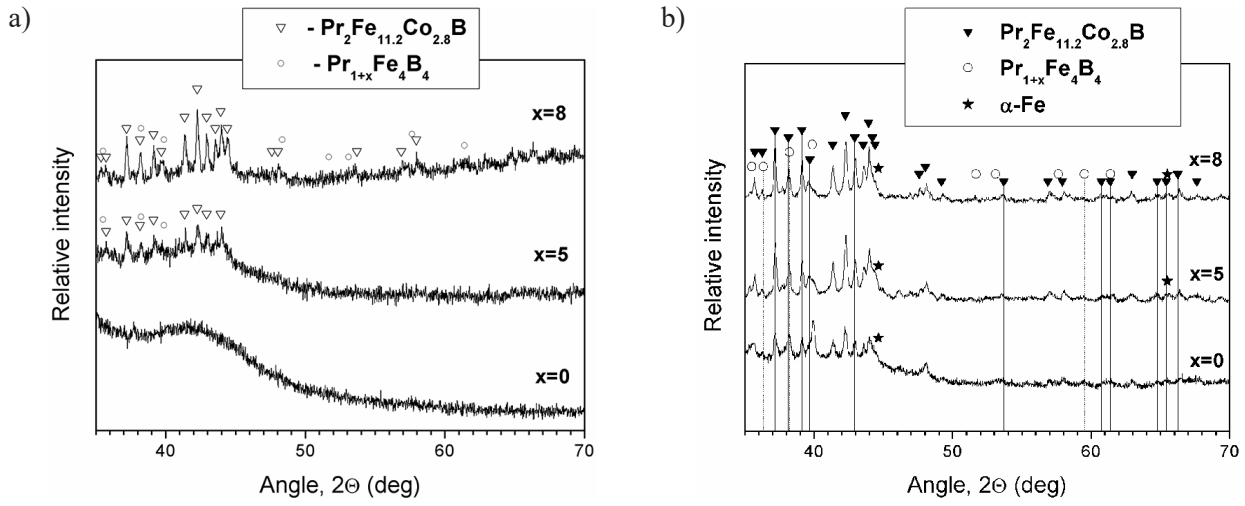


**Fig. 1.** XRD patterns measured for the 1-mm diameter rods of $Pr_9Fe_{50+x}Co_{13}Zr_1Nb_4B_{23-x}$ (x = 0, 5, 8) alloys in the as-cast state (a) and subjected to annealing at 983 K for 5 min (b)

**TABLE 1**

Rietveld refinement results; refined cell parameters (a, c), crystallite sizes (d) and weight fraction (wt. %) of crystalline phases (2:14:1 – $Pr_2Fe_{11.2}Co_{2.8}B$, 1:4:4 – $Pr_{1+x}Fe_4B_4$, α-Fe) and amorphous phase

| at. % of Fe | phase | a [nm] | c [nm] | d [nm] | wt. [%] |
|---|---|---|---|---|---|
| 50 (annealed) | 2:14:1 | 0.8774 ± 0.0001 | 1.2149 ± 0.0002 | 35.0 ± 0.6 | 56.3 ± 0.7 |
| | 1:4:4 | 0.7099 ± 0.0001 | 3.4942 ± 0.0012 | 17.3 ± 0.6 | 36.6 ± 0.6 |
| | α-Fe | 0.2868 ± 0.0001 | – | 10.1 ± 0.5 | 7.1 ± 0.3 |
| 55 (as-cast) | 2:14:1 | 0.8811 ± 0.0001 | 1.2247 ± 0.0002 | 31.1 ± 1.1 | 33.6 ± 0.6 |
| | 1:4:4 | 0.7164 ± 0.0002 | 3.5073 ± 0.0011 | 14.4 ± 0.8 | 15.3 ± 0.4 |
| | amorphous | – | – | – | 51.1 ± 0.7 |
| 55 (annealed) | 2:14:1 | 0.8774 ± 0.0001 | 1.2171 ± 0.0002 | 55.1 ± 0.9 | 38.9 ± 0.7 |
| | 1:4:4 | 0.7107 ± 0.0001 | 3.4820 ± 0.0010 | 25.3 ± 0.9 | 49.4 ± 0.7 |
| | α-Fe | 0.2873 ± 0.0001 | – | 8.7 ± 05 | 11.7 ± 0.4 |
| 58 (as-cast) | 2:14:1 | 0.8799 ± 0.0001 | 1.2241 ± 0.0002 | 55.7 ± 1.2 | 25.5 ± 0.6 |
| | 1:4:4 | 0.7128 ± 0.0001 | 3.4918 ± 0.0012 | 21.4 ± 0.7 | 23.7 ± 0.6 |
| | amorphous | – | – | – | 50.8 ± 0.7 |
| 58 (annealed) | 2:14:1 | 0.8756 ± 0.0001 | 1.2150 ± 0.0002 | 97.6 ± 1.7 | 39.7 ± 0.7 |
| | 1:4:4 | 0.7084 ± 0.0001 | 3.4784 ± 0.0012 | 33.1 ± 1.2 | 45.5 ± 0.7 |
| | α-Fe | 0.2867 ± 0.0001 | – | 12.3 ± 0.5 | 14.8 ± 0.4 |

talline phases are collected in Table 1. The XRD studies have shown that the $Pr_9Fe_{50}Co_{13}Zr_1Nb_4B_{23}$ alloy rods were fully amorphous. An increase in the Fe content (x = 5, 8) caused the precipitation of crystalline phases within the amorphous matrix during rapid solidification. By using the Rietveld-PONKCS method, it has been established that about 50 wt.% of the amorphous phase was present in their phase constitution. It implies the reduction of the GFA with the decrease in B content. These results are consistent with those obtained for the 0.5-mm and 1-mm thick suction-cast plates manufactured for the same alloy compositions [6, 13]. The identification of precipitating phases was restricted by low intensities of diffraction peaks.

However, for the as-cast rods of higher Fe contents (55 and 58 at.% of Fe), the phase analysis revealed the presence of the hard magnetic $Pr_2Fe_{11.2}Co_{2.8}B$ (2:14:1) and the paramagnetic $Pr_{1+x}Fe_4B_4$ (1:4:4) phases. The amounts of constituent crystalline phases differ in x = 5 and x = 8 as-cast rods as was shown in Table 1. This is reflected in their magnetic properties (Fig. 3a). The coercivity ${}_JH_c$ is higher for the x = 5 alloy, then for the x = 8, which might be related to a higher amount of the hard magnetic 2:14:1 phase in the x = 5 alloy (∼34 wt.% of the 2:14:1 phase) than in the x = 8 as-cast rods (∼25 wt.%). The amount of the paramagnetic 1:4:4 phase also differs in both as-cast rods. Its amount is lower in the case of the x = 5 alloy (∼15 wt.% of the 1:4:4 phase) than in the x = 8 alloy (∼24 wt.% of the 1:4:4 phase). Based on these results, one can conclude that higher magnetic polarization $J_s$ (measured at the maximum magnetic field) for the x = 8 alloy than this for x = 5 alloy is related to the different chemical composition of the amorphous phase in both as-cast rods (higher Fe content in the amorphous phase of the x = 8 alloy). Furthermore, the sizes of crystallites precipitating during rapid solidification are larger for specimens with lower B content. One can conclude that for the investigated alloy the boron element has an important role in the glass formation during the rapid solidification process. Short-time annealing (at 983 K for 5 min) led to nucleation and growth of crystalline phases in all rod specimens. However, the presence of crystalline phases in the as-cast rods had a significant impact on the weight fractions of constituent phases in the samples subjected to annealing. The differences in the phase constitution between as-cast and annealed rods come out in the fractions of constituent phases. Annealing at 985 K resulted in the full crystallization of the investigated samples. The phase analysis has shown the presence of hard magnetic $Pr_2Fe_{11.2}Co_{2.8}B$ and paramagnetic $Pr_{1+x}Fe_4B_4$ phases in all annealed specimens, similarly to the as-cast x = 5 and x = 8 rods. Furthermore, an additional α-Fe phase was identified for all specimens. The diffraction peaks coming from the α-Fe phase are visible as weak humps on the right-hand slopes of the XRD patterns measured for the x = 8 and x = 5 alloys (Fig. 1b). However, based on the TEM studies (Fig. 2), the microstructure of the investigated specimens is very fine-grained, with nanocrystals having sizes lower than 100 nm. Such a microstructure leads to the substantial widening of the diffraction peaks. Furthermore, the multiphase composition of the studied specimens has a certain impact on the XRD pattern. Especially, the lines coming from the α-Fe phase are widened and overlap with those coming from the hard magnetic 2:14:1 and paramagnetic 1:4:1 phases, whose corresponding peaks are also widened. This fact was considered in the Rietveld refinement model that was used in these studies. The results of the Rietveld refinement are consistent with the magnetic measure-

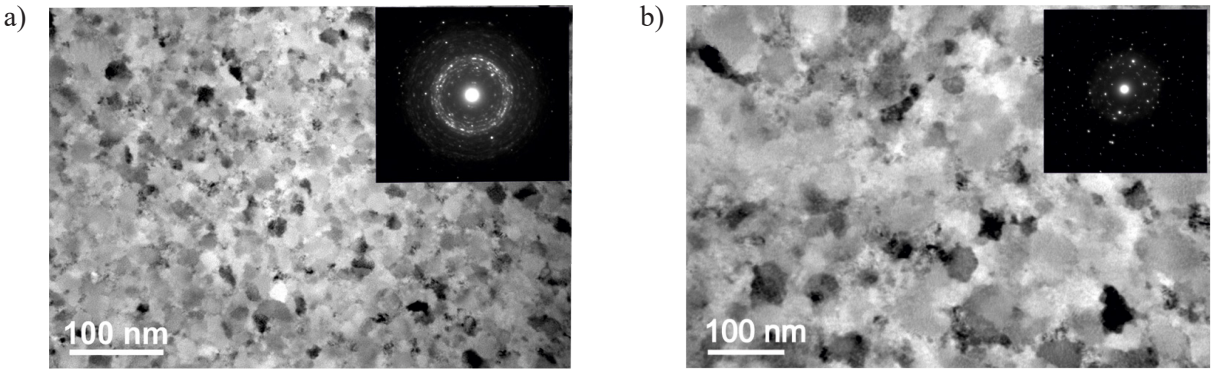


**Fig. 2.** Transmission electron microscopy images obtained for the annealed 1-mm diameter rods of the $Pr_9Fe_{50}Co_{13}Zr_1Nb_4B_{23}$ (a) and $Pr_9Fe_{58}Co_{13}Zr_1Nb_4B_{15}$ (b) alloys

ments where the increase of the Fe contents in the alloy composition resulted in the rise of the magnetic moments of the annealed specimens. Here the presence of the α-Fe phase is responsible for the higher magnetic polarization of x = 5 and x = 8 rods at high magnetic fields. The highest amount of the hard magnetic 2:14:1 phase was determined for the x = 0 alloy (Table 1). In the case of annealed x = 5 and x = 8 alloy rods, a moderate increase in the weight fraction of the 2:14:1 phase was found. Furthermore, an increase in the crystallite sizes of the 2:14:1 phase in both alloys suggests that annealing causes the growth of the crystallites that already precipitated during the rapid solidification rather than nucleation and growth of this phase. On the other hand, a moderate increase in the crystallite sizes and the rise of weight fraction of the paramagnetic phase imply extremely intensive nucleation and growth of the paramagnetic 1:4:4 and soft magnetic α-Fe phases during annealing. It should be mentioned that the lattice parameters determined for all investigated specimens using the Rietveld refinement were not significantly different for particular phases.

The transmission electron microscopy (TEM) images obtained for the annealed 1-mm diameter rods of the $Pr_9Fe_{50}Co_{13}Zr_1Nb_4B_{23}$ and $Pr_9Fe_{58}Co_{13}Zr_1Nb_4B_{15}$ alloys are shown in Figs. 2a and 2b, respectively. A relatively uniform microstructure was observed for the rod of the $Pr_9Fe_{50}Co_{13}Zr_1Nb_4B_{23}$ alloy where the average grain diameters of 20–40 nm were measured. Furthermore, the dotted ring-shaped electron diffraction, confirms a crystalline microstructure of the specimen. For the rod of the $Pr_9Fe_{58}Co_{13}Zr_1Nb_4B_{15}$ alloy, an inhomogeneous microstructure, consisting of coarse nanocrystals (dia. ∼100 nm) mixed with finer ones, was observed (Fig. 2b). Such a distinct microstructure came from the growth of the crystallites formed during the rapid solidification of rods and subsequent nucleation and growth of new crystallites during annealing. The measured crystallite sizes are in good agreement with those obtained from the XRD studies.

The hysteresis loops measured for the as-cast and annealed rods of $Pr_9Fe_{50+x}Co_{13}Zr_1Nb_4B_{23-x}$ alloys are shown in Fig. 3. For the as-cast rods of the x = 0 alloy, the $J(H)$ curve is typical for the soft magnetic material that confirms its amorphous structure. It is characteristic for these types of alloys that fully amorphous samples exhibit significantly larger polarizations than the crystalline ones in the available external magnetic fields (of ∼2T) [6]. One must notice that in the annealed x = 0 rods the 2:14:1 phase is present. This phase has relatively low saturation polarization (∼1.67T for pure 2:14:1 phase at room temperature) and a high anisotropy field ($\mu_0 H_A = 8.7$T). Furthermore, the isotropic crystallization of this hard magnetic phase occurs during the annealing of the alloy. For this reason,

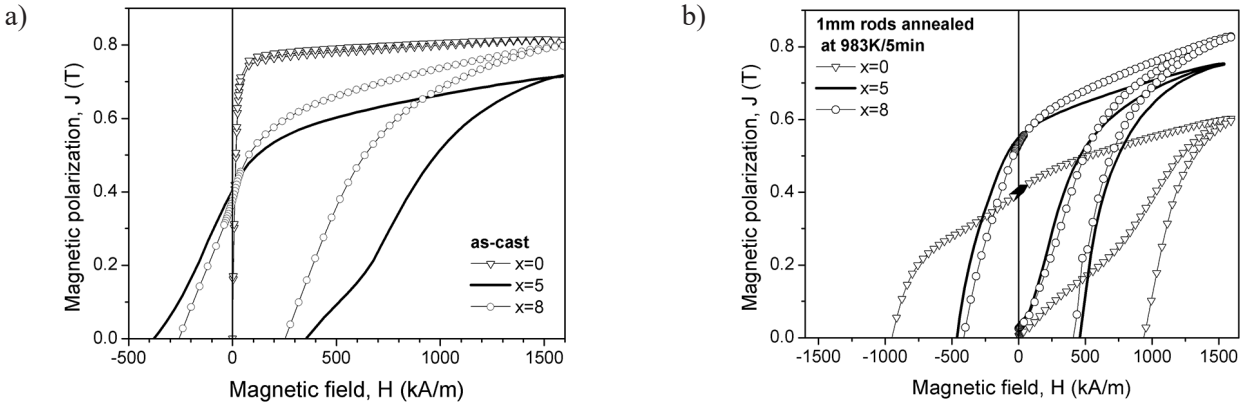


**Fig. 3.** The hysteresis loops measured for 1-mm diameter rods of $Pr_9Fe_{50+x}Co_{13}Zr_1Nb_4B_{23-x}$ (x = 0, 5, 8) alloys in the as-cast state (a) and after annealing at 983 K for 5 min (b)

the maximum applied magnetic field does not saturate the sample, thus the resultant magnetization measured below ~2T is relatively low for the crystalline specimen. As the amorphous sample is initially soft magnetic, therefore it can be saturated at low magnetic fields, reaching much higher magnetic polarizations in the available range of external magnetic fields.

An increase in the Fe content to 55 at.% caused a decrease in glass-forming abilities, leading to the growth of the hard magnetic and paramagnetic phases during the rapid solidification, which was confirmed by XRD studies. Consequently, the as-cast rods had hard magnetic properties with relatively high coercivity of ~370 kA/m. As was expected based on the XRD studies, the annealing caused significant a change in the hysteresis loops measured for the rods of various composition. All annealed samples revealed the remanence enhancement, $J_r/J_s$, reaching up to 0.70 for the rods containing 55 at.% of Fe.

Changes in the saturation polarization $J_s$, remanence $J_r$, coercivity ${}_JH_c$ and maximum magnetic energy product $(BH)_{max}$ with the alloy composition for the annealed rod samples are shown in Fig. 4. A gradual decrease of coercivity ${}_JH_c$ from 950 kA/m (for 50 at.% of Fe) to about 400 kA/m (for 58 at.% of Fe) is most likely related to the decrease of the weight fraction of the hard magnetic 2:14:1 phase. The highest coercivity ${}_JH_c$ value was measured for the sample with very fine and uniform crystallites of a hard magnetic phase. The $J_r$ and $(BH)_{max}$ reached the highest values for the annealed rod of 55 at.% of Fe alloy. This might be related to the impact of the α-Fe phase. Relatively low crystallite sizes of this soft magnetic phase may contribute to the exchange spring effect in these hard magnetic materials [18]. However, a relatively low weight fraction of the hard magnetic phase for the annealed rods of the x = 5 and x = 8 alloy did not produce the expected outcomes of the exchange spring effect.

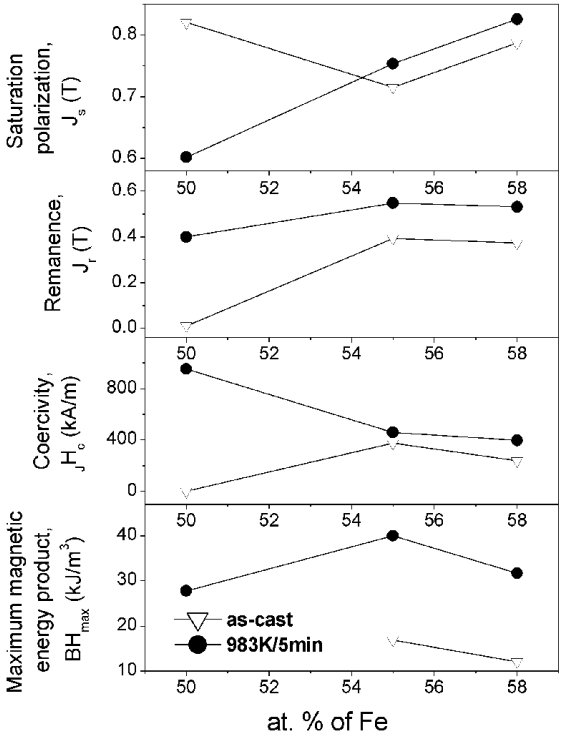


**Fig. 4.** Dependences of the remanence polarization $J_r$, coercivity field ${}_JH_c$ and maximum magnetic energy product $(BH)_{max}$ in the alloy composition measured for the 1-mm dia. rods of $Pr_9Fe_{50+x}Co_{13}Zr_1Nb_4B_{23-x}$ (x = 0, 5, 8) alloys in as-cast state and after annealing at 983 K for 5 min

The influence of the microstructure and phase constitution on the magnetization reversal process in the annealed rods can be investigated based on the profiles of the switching field distribution (SFD) curves. This distribution is defined as the function of derivatives of the irreversible remanence magnetization with respect to the magnetic field $dM_{irr}/dH$ vs. the value of magnetic field $H$. The SFD curves were calculated from recoil curves measured on the specimens in the demagnetized state and correspond to the rates of magnetic remanence $M_{irr}$ changes with the increase in the maximum applied magnetic fields $H$ [19–23]. The profile of the SFD curve provides information about the strength of magnetic interactions between grains of magnetic phases. Therefore, a sharp and narrow peak in the SFD indicates a well-coupled magnetic system of homogenous grains, while broad distribution corresponds to a low level of magnetic coupling [24]. Broad SFD curves calculated for all annealed samples carried out in the present studies suggest weak coupling of hard magnetic grains in the annealed rods (Fig. 5). However, for the x = 0 alloy rods, the homogenous microstructure

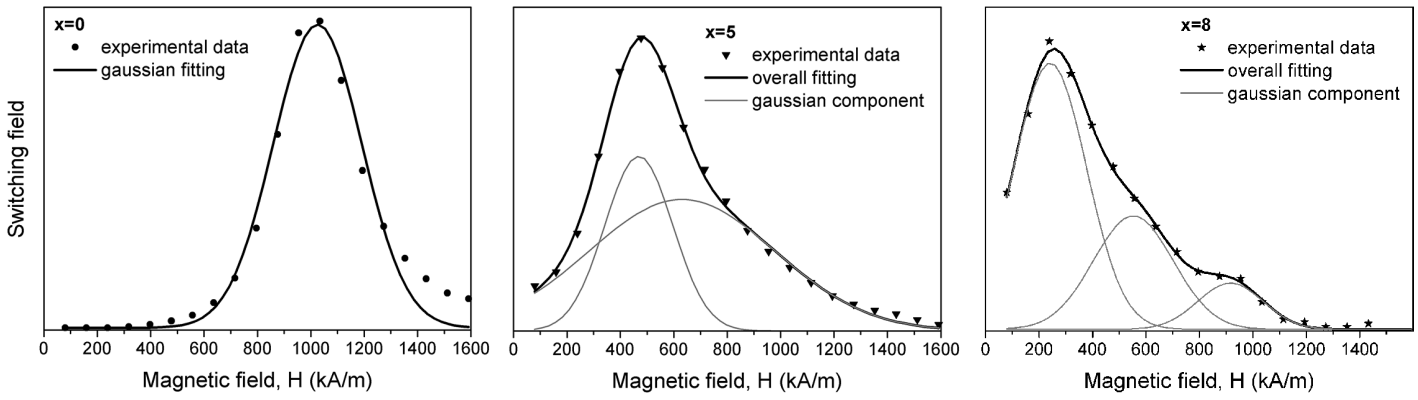


**Fig. 5.** The switching field distributions (SFD) for the annealed 1-mm diameter rods of the $Pr_9Fe_{50+x}Co_{13}Zr_1Nb_4B_{23-x}$ (x = 0, 5, 8) alloys

consisting of single-domain grains resulted in a Gaussian distribution of switching fields, with a maximum ($H_{max}$) at about 1000 kA/m, which is close to the ${}_JH_c$ of the sample. On the other hand, for the x = 5 and x = 8 annealed rods, a characteristic tail at high magnetic fields (above 800 kA/m) was shown. That can be attributed to the inhomogeneous microstructure of the samples. For these specimens the SFD curves were fitted with two or three Gaussian distributions. The positions of SFD maxima ($H_{max}$) are collected in Table 2. Variation of the grain sizes for alloys of higher Fe content caused their magnetization reversal in wide range of magnetic fields. The Gaussian deconvolution of SFD curves gives additional components with maxima at lower magnetic fields, at which larger grains are reversed, although some fraction of grains is still reversed at higher fields. The evolution of SFD shapes implies changes in the fraction of single and multi-domain grains with an increase in the Fe content in the alloy composition.

**TABLE 2**

The parameters of the Gaussian fitting of SFD curves: $H_{max}$ — the value of magnetic field at which the maximum in $dM_{irr}/dH$ occurs, $W_H$ — the half width of Gaussian curve

| | $H_{max}$ [kA/m] | $W_H$ [kA/m] |
|---|---|---|
| 50 at. % Fe | 1025 | 408 |
| 55 at. % Fe | 468<br>630 | 315<br>795 |
| 58 at. % Fe | 241<br>552<br>916 | 370<br>403<br>308 |

In order to describe the inter-granular interactions in the annealed rods, the δM plots can also be used. The δM was defined by the formula [21]:

$$\delta M(H) = \frac{M_{irr}^{D}(H) - \left(M_r - 2M_{irr}^{R}(H)\right)}{M_r}. \qquad (1)$$

where: $M_r$ – remanence magnetization; $M_{irr}^{D}(H)$ – demagnetization remanence measured after applying the demagnetizing magnetic field $H$ to the sample in magnetic saturation; $M_{irr}^{R}(H)$ – magnetization remanence measured after applying a magnetizing field $H$ to the initially demagnetized sample. $\delta M(H)$ reaches zero for noninteracting particles based on Wohlfarth's model [25]. The values of $M_{irr}^{D}(H)$ and $M_{irr}^{R}(H)$ used in this procedure can also be determined from the recoil curves. Based on the Kelly *et al*. [26] interpretation, the non-zero positive $\delta M$ corresponds to exchange interactions that can stabilize magnetization, while the negative $\delta M$ can be attributed to dipolar interactions that demagnetize the sample. The $\delta M$ plots calculated for the annealed samples are presented in Fig. 6. The strongest exchange interactions, as indicated by positive $\delta M$ values, were present for the annealed rods of the x = 0 alloy in a wide range of magnetic fields up to 1100 kA/m. For this sample, the $\delta M$ changes its sign at ~1100 kA/m, which indicates a dominant role of demagnetizing interactions between grains at high magnetic fields. In the case of x = 5 and x = 8 alloy rods, a lower positive $\delta M$ values in magnetic fields up to 600 kA/m were measured. In higher fields, the $\delta M$ is close to zero, which can indicate a similar contribution of exchange and dipolar interactions to the magnetization of the samples.

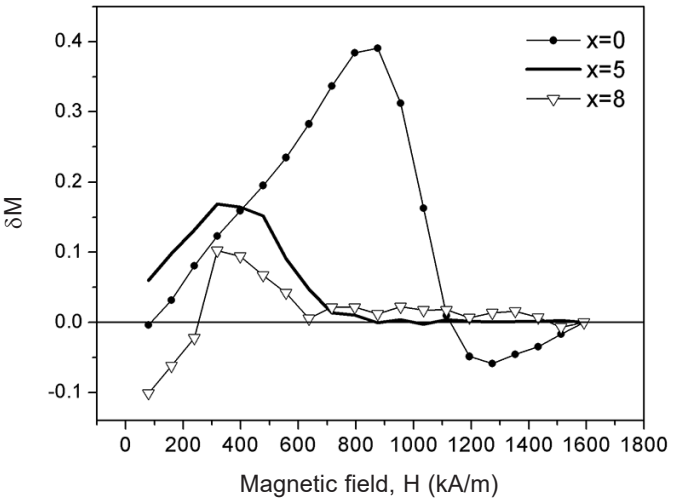


**Fig. 6.** The $\delta M$ plots for the annealed 1-mm diameter rods of the $Pr_9Fe_{50+x}Co_{13}Zr_1Nb_4B_{23-x}$ (x = 0, 5, 8) alloys

## 4. CONCLUSIONS

It was shown by the XRD studies that glass forming abilities of $Pr_9Fe_{50+x}Co_{13}Zr_1Nb_4B_{23-x}$ ($x$ = 0, 5, 8) alloys decrease with an increase in the Fe content. The x = 0 alloy rods in as-cast state were fully amorphous, while higher Fe content resulted in the precipitation of the hard magnetic $Pr_2Fe_{11.8}Co_{2.8}B$ and paramagnetic $Pr_{1+x}Fe_4B_4$ phases within the amorphous matrix. The phase constitution of the as-cast samples undoubtedly affected the final phase composition and magnetic properties of the rods subjected to annealing. The initial state of rods also influenced the microstructure of the annealed specimens. Heat treatment of fully amorphous rods of the x = 0 alloy resulted in the formation of a homogenous microstructure consisting of nanocrystals of diameters between 20–40 nm. This fact and a large fraction of the hard magnetic phase resulted in the highest coercivity of these alloy rods. Partial crystallization of as-cast specimens produced for alloys of higher Fe contents caused the formation of an inhomogeneous microstructure during annealing. However, the highest $J_r$ and $(BH)_{max}$ were achieved for the annealed rods of $Pr_9Fe_{55}Co_{13}Zr_1Nb_4B_{18}$ alloy, which might be related to the presence of the α-Fe phase responsible for larger saturation polarization. Relatively low crystallite sizes of this soft magnetic phase may contribute to the exchange spring effect in these hard magnetic materials. It was shown that the increase in B content (at the expense of Fe) in the chemical composition of the alloy promoted the formation of the paramagnetic phase during annealing. Furthermore, a higher B to Fe ratio together with Zr and Nb additions hindered the crystal growth. Broad switching field distributions reflecting a wide range of magnetic fields that

cause the magnetization reversal are related to the inhomogeneity of the microstructure. The $\delta M$ plots have shown that the strongest exchange interactions between grains occur for the annealed rods of the x = 0 alloy with the finest crystallites. For samples with coarser crystallites existence of multi-domain structure and dipolar interactions, it causes the reduction of $\delta M$ values.

## REFERENCES

[1] A. Łebkowski, "A way of neodymium-iron-boron magnets regeneration in surface-mounted PMSM used in electric vehicles", *Bull. Pol. Acad. Sci. Tech. Sci.*, vol. 65, no. 5, pp. 751–758, 2017, doi: 10.1515/bpasts-2017-0081.

[2] S. Hirosawa, H. Kanekiyo, Y. Shigemoto, and T. Miyoshi, in *Proceedings of 18th International Workshop on High Performance Magnets and Their Applications*, 2004, pp. 655–666.

[3] P. Pawlik, K. Pawlik, H.A. Davies, J.J. Wysocki, and W. Kaszuwara, "Nanocrystalline (Pr, Dy)-(Fe, Co)-Zr-Ti-B magnets produced directly by rapid solidification," *J. Phys. Conf. Ser.*, vol. 144, pp. 1–5, 2009, doi: 10.1088/1742-6596/144/1/012060.

[4] J. Zhang, K.Y. Lim, Y.P. Feng, and Y. Li, "Fe-Nd-B-based hard magnets from bulk amorphous precursor," *Scr. Mater.*, vol. 56, no. 11, pp. 943–946, Jun. 2007, doi: 10.1016/j.scriptamat.2007.02.016.

[5] X. Bao, J. Zhu, W. Li, X. Gao, and S. Zhou, "Influence of zirconium addition on microstructure, magnetic properties and thermal stability of nanocrystalline $Nd_{12.3}Fe_{81.7}B_{6.0}$ alloy," *J. Rare Earths*, vol. 27, no. 5, pp. 843–847, Oct. 2009, doi: 10.1016/S1002-0721(08)60347-6.

[6] K. Pawlik, P. Pawlik, J.J. Wysłocki, and W. Kaszuwara, "Structural and magnetic studies of bulk nanocomposite magnets derived from rapidly solidified Pr-(Fe,Co)-(Zr,Nb)-B alloy," *Materials*, vol. 13, no. 7, pp. 1–16, 2020, doi: 10.3390/ma13071515.

[7] W. Zhang and A. Inoue, "Bulk nanocomposite permanent magnets produced by crystallization of (Fe,Co)-(Nd,Dy)-B bulk glassy alloy," *Appl. Phys. Lett.*, vol. 80, no. 9, pp. 1610–1612, Mar. 2002, doi: 10.1063/1.1456259.

[8] Y. Long, W. Zhang, X. Wang, and A. Inoue, "Effects of transition metal substitution on the glass-formation ability and magnetic properties of $Fe_{62}Co_{9.5}Nd_3Dy_{0.5}B_{25}$ glassy alloy," *J. Appl. Phys.*, vol. 91, no. 8, pp. 5227–5229, Apr. 2002, doi: 10.1063/1.1457538.

[9] H.W. Chang *et al.*, "Magnetic properties, phase evolution and microstructure of directly quenched bulk Pr-Fe-B-Nb magnets," *Scr. Mater.*, vol. 59, no. 2, pp. 227–230, Jul. 2008, doi: 10.1016/j.scriptamat.2008.03.011.

[10] I. Betancourt and H.A. Davies, "Influence of Zr and Nb dopant additions on the microstructure and magnetic properties of nanocomposite $RE_2(Fe,Co)_{14}B/\alpha(Fe,Co)$ (RE = Nd-Pr) alloys," *J. Magn. Magn. Mater.*, vol. 261, no. 3, pp. 328–336, May 2003, doi: 10.1016/S0304-8853(02)00366-9.

[11] P. Pawlik and H.A. Davies, "Glass formability of Fe-Co-Pr-Dy-Zr-B alloys and magnetic properties following devitrification," *Scr. Mater.*, vol. 49, no. 8, pp. 755–760, Oct. 2003, doi: 10.1016/S1359-6462(03)00428-7.

[12] K. Pawlik, P. Pawlik, W. Kaszuwara, and J.J. Wysłocki, "Glass forming abilities and crystallization process in amorphous Pr-Fe-Co-Zr-Nb-B alloys of various B content," in *Acta Physica Polonica A*, vol. 131, no. 4, pp. 979–981, Apr. 2017, doi: 10.12693/APhysPolA.131.979.

[13] K. Pawlik, P. Pawlik, and J. J. Wysłocki, "The Bulk Glass Forming Ability and Magnetic Properties of $Pr_9Fe_{50+x}Co_{13}Zr_1Nb_4B_{23-x}$ (x = 0, 2, 5, 8) Alloys," *Acta Phys. Pol. A*, vol. 118, no. 5, pp. 900–902, 2010.

[14] P. Pawlik, K. Pawlik, and A. Przybył, "Investigation of the cooling rate in the suction casting process," *Rev. Adv. Mater. Sci*, vol. 18, pp. 81–84, 2008, [Online]. Available: https://www.researchgate.net/publication/285013213 (Accessed: Feb. 10, 2021).

[15] K. Pawlik, P. Pawlik, J.J. Wysłocki, and W. Kaszuwara, "Microstructure and magnetic interactions in Pr-Fe-Co-Zr-Nb-B magnets," *J. Alloys Compd.*, vol. 536, no. SUPPL.1, pp. S348–S353, Sep. 2012, doi: 10.1016/j.jallcom.2011.12.003.

[16] P. Pawlik, H.A. Davies, and M.R.J. Gibbs, "Magnetic properties and glass formability of $Fe_{61}Co_{10}Zr_5W_4B_{20}$ bulk metallic glassy alloy," *Appl. Phys. Lett.*, vol. 83, no. 14, pp. 2775–2777, 2003, doi: 10.1063/1.1614419.

[17] K. Pawlik, "Effect of heat treatment on the phase transformation and magnetic properties of the rapidly solidified $Pr_9Fe_{58}Co_{13}Zr_1Nb_4B_{15}$ alloy ribbons," *Acta Phys. Pol. A*, vol. 131, no. 5, pp. 1264–1269, 2017, doi: 10.12693/APhysPolA.131.1264.

[18] E.F. Kneller and R. Hawig, "The exchange-spring magnet: A new material principle for permanent magnets," *IEEE Trans. Magn.*, vol. 27, no. 4, pp. 3588–3600, 1991, doi: 10.1109/20.102931.

[19] P.I. Mayo, R.M. Erkkila, A. Bradbury, and R.W. Chantrell, "Interaction Effects in Longitudinally Oriented and Non-Oriented Barium Hexaferrite Tapes," *IEEE Trans. Magn.*, vol. 26, no. 5, pp. 1894–1896, 1990, doi: 10.1109/20.104560.

[20] B.E. Meacham, D.J. Branagan, and J.E. Shield, "Understanding the link between nanoscale microstructural features and dynamic hysteresis phenomena," *J. Magn. Magn. Mater.*, vol. 277, no. 1–2, pp. 123–129, Jun. 2004, doi: 10.1016/j.jmmm.2003.10.034.

[21] S. Aich and J.E. Shield, "A study on the order-disorder phase transformations of rapidly solidified Sm-Co-based permanent magnets," *J. Magn. Magn. Mater.*, vol. 313, no. 1, pp. 76–83, Jun. 2007, doi: 10.1016/j.jmmm.2006.12.006.

[22] M. Fearon, R.W. Chantrell, and E.P. Wohlfarth, "A theoretical study of interaction effects on the remanence curves of particulate dispersions," *J. Magn. Magn. Mater.*, vol. 86, no. 2–3, pp. 197–206, May 1990, doi: 10.1016/0304-8853(90)90121-6.

[23] J.E. Shield, B.B. Kappes, D.J. Branagan, and J. Bentley, "Chemical partitioning during crystallization and its effect on the microstructure and magnetic behavior of modified Nd-Fe-B permanent magnets," *J. Magn. Magn. Mater.*, vol. 246, no. 1–2, pp. 73–79, Apr. 2002, doi: 10.1016/S0304-8853(02)00028-8.

[24] H. Chiriac, M. Marinescu, P. Tiberto, and F. Vinai, "Reversible magnetization behavior and exchange coupling in ttwo-phase NdFeB melt spun ribbons," *Mater. Sci. Eng. A*, vol. 304–306, no. 1–2, pp. 957–960, May 2001, doi: 10.1016/S0921-5093(00)01599-9.

[25] E.P. Wohlfarth, "Relations between different modes of acquisition of the remanent magnetization of ferromagnetic particles," *J. Appl. Phys.*, vol. 29, no. 3, pp. 595–596, Mar. 1958, doi: 10.1063/1.1723232.

[26] P.E. Kelly, K. O'Grady, P.L. Mayo, and R.W. Chantrell, "Switching mechanisms in cobalt-phosphorus thin films," *IEEE Trans. Magn.*, vol. 25, no. 5, pp. 3881–3883, 1989, doi: 10.1109/20.42466.